Universiteit
Leiden
The Netherlands

# Surface-structure dependence of water-related adsorbates on platinum

Badan, C.

**Citation**

Badan, C. (2016, November 22). *Surface-structure dependence of water-related adsorbates on platinum*. Retrieved from https://hdl.handle.net/1887/44295

| | |
|---|---|
| Version: | Not Applicable (or Unknown) |
| License: | Licence agreement concerning inclusion of doctoral thesis in the Institutional Repository of the University of Leiden |
| Downloaded from: | https://hdl.handle.net/1887/44295 |

**Note:** To cite this publication please use the final published version (if applicable).

Cover Page

Universiteit Leiden

The handle http://hdl.handle.net/1887/44295 holds various files of this Leiden University dissertation.

**Author**: Badan, C.
**Title**: Surface-structure dependence of water-related adsorbates on platinum
**Issue Date**: 2016-11-22

# Chapter 2

# The Analysis of Temperature Programmed Desorption Experiments

## 2.1 Temperature Programmed Desorption (TPD)

TPD is one of the most common techniques in surface science and heterogeneous catalysis. With TPD, desorbed species from a sample can be detected by a quadrupole mass spectrometer (QMS) while the temperature of the sample increases with time. It can provide, amongst others, information regarding the binding energy of the bound species, desorption kinetics, surface coverage and reaction order[1]. The rate of desorption of an adsorbate is given by the following general equation:

$$\mathrm{r}(\theta) = -\frac{\mathrm{d}\theta}{\mathrm{dt}} = \nu_{des}\theta^{\mathrm{n}}\exp(-E_{des}/RT) \tag{2.1}$$

$$\mathrm{T} = \mathrm{T}_0 + \beta t \tag{2.2}$$

r = rate of desorption
$\theta$ = coverage in monolayers ($ML$)
$\nu_{des}$ = prefactor
n = order of desorption
$E_{des}$ = activation energy for desorption
R = gas constant
T = temperature ($K$)
$\mathrm{T}_0$ = initial temperature

$\beta$ = heating rate
t = time

If the rate of the desorption into the UHV chamber is lower than the pumping speed of vacuum system, the desorption rate is proportional to the pressure rise in the chamber. In a TPD spectrum, the integrated QMS signal is proportional to the amount of adsorbates on the surface and the shape of the desorption feature contains information about the kinetics parameters, including lateral interactions. Although this technique is very simple, cheap and applicable to real crystals, obtaining a high quality spectrum is rather difficult. Also, the interpretation of the data requires meticulous analysis for extracting kinetic information.

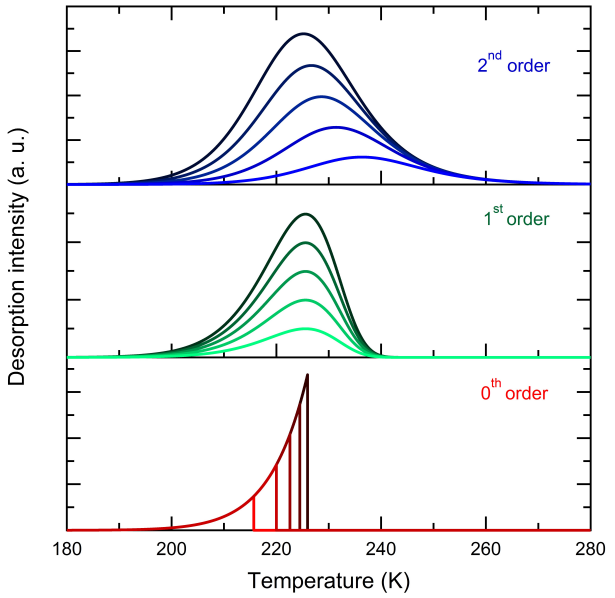


Figure 2.1: Simulated temperature programmed desorption spectra of adsorbed species for initial coverages of 0.2, 0.4, 0.6, 0.8 and 1.0 ML. Top, middle and bottom sections show the second, first and zeroth order desorption, respectively. For each simulation, the activation energy and prefactor are fixed at 60 kJ/mol and 1x10$^{13}$ s$^{-1}$, respectively.

In figure 2.1, we simulated various TPD spectra at 0.2, 0.4, 0.6, 0.8 and 1.0 ML coverages using rate equation 2.1. Top, middle and bottom sections show second, first and zeroth order of desorption kinetics. For each simulation we set the $E_{des}$ and prefactor at 60 kJ/mol and 1x10$^{13}$ s$^{-1}$, respectively. In the simulations, the lateral interactions between adsorbed species are ignored.

Zero-order desorption kinetics, for which the rate increases exponentially with temperature and the onsets have a common leading edge, imply a coverage independent desorption rate (bottom panel in figure 2.1). Species which follow zero-order kinetics have a constant coverage and are replenished by another state during desorption. The desorption of water multilayers from clean Pt(111) surfaces is a very well-known example of a zero-order desorption kinetics. For first order desorption kinetics, the rate is proportional to instantaneous coverage and temperature of the peak at maximum desorption rate ($T_M$) does not increase with increasing coverage (middle panel in figure 2.1). Generally, non-dissociative molecular, e.g., water desorption from Pt(111) terraces at sub-monolayer coverages[2–4], and atomic adsorption, e.g., Xe desorption from graphene[5], yield first order desorption kinetics. For reactions that follow second order desorption kinetics, the rate is proportional to $\theta^2$ (top panel in figure 2.1). With increasing coverage, the peak temperature shifts to lower values while the peaks follow common trailing edges. Molecules that dissociatively-adsorb, e.g., $H_2$ and $O_2$[3], on the substrates, generally follow second order desorption kinetics. In the absence of lateral interactions and for well-mixed adlayers, equation 2.1 generally yields accurate results for simple desorption reactions. However, in many adsorption systems lateral interactions between the adsorbates exist. The presence of repulsive or attractive interactions not only make $\nu_{des}$ and $E_{des}$ coverage dependent, they can also change the reaction order[6, 7]. Furthermore, the desorption order does not have to be an integer[8] and a TPD spectrum may contain a combination of different desorption orders [9, 10]. To extract accurate kinetic information from TPD spectra, various methods have been developed[7, 11, 12]. In the following sections, some of the most common analysis techniques are discussed.

### 2.1.1 Redhead analysis

The Redhead analysis[13] is based on the calculation of the activation energy for desorption from the temperature of the peak at maximum desorption rate. Redhead assumed that kinetic parameters are independent of surface coverage and desorption follows first order kinetics. For this method, a very good estimation of the prefactor, $\nu_{des}$, is crucial. Therefore, it is only useful to determine $E_{des}$ when the prefactor is reasonably well known (equation 2.5).

To obtain the Redhead equation, equations 2.1 and 2.2 can be expressed in the following way.

$$\frac{r}{\beta} = \frac{d\theta}{dT} = \frac{\nu_n}{\beta}\theta^n exp(-E_{des}/RT) \tag{2.3}$$

$$\frac{E_{des}}{RT_M} = ln\left(\frac{\nu_n T_M n\theta_M^{n-1}}{\beta}\right) - ln\frac{E_{des}}{RT_M} \tag{2.4}$$

where:
n = 1, and $E_{des} \cong 0.25\ T_M$

$$E_{des} = RT_M[ln(\nu_{des}T_M/\beta) - 3.46] \tag{2.5}$$

### 2.1.2 Leading edge analysis

This method was introduced by Habenschaden and Küppers[14] and allows the extraction of coverage- and temperature-dependent activation parameters. This method only uses the onset of a TPD spectrum. An Arrhenius plot, ln(r) versus 1/T, yields -$E_{des}$ (slope) and the prefactor (intercept).

Table 2.1: The obtained desorption energies (kJ/mol) and prefactors ($s^{-1}$) from leading edge (LE) analysis and Redhead analysis at 0.2, 0.4, 0.6, 0.8 and 1.0 ML. For the simulations, $E_{des}$ and prefactors are set to 60 kJ/mol and 1.0x$10^{13}$ $s^{-1}$, respectively. For extracting the $E_{des}$ from the Redhead equation, the prefactors are set to 1.0x$10^{13}$ $s^{-1}$.

| Method | $\theta$ (ML) | Zero order | | First order | | Second order | |
|---|---|---|---|---|---|---|---|
| | | $E_{des}$ | $\nu_{des}$ | $E_{des}$ | $\nu_{des}$ | $E_{des}$ | $\nu_{des}$ |
| LE | 0.2 | 60.0 | 1.0x$10^{13}$ | 60.0 | 1.0x$10^{13}$ | 60.0 | 1.0x$10^{13}$ |
| Redhead | | 59.7 | — | 60.0 | — | 62.9 | — |
| LE | 0.4 | 60.0 | 1.0x$10^{13}$ | 60.0 | 8.0x$10^{12}$ | 60.0 | 6.4x$10^{12}$ |
| Redhead | | 58.5 | — | 60.0 | — | 61.6 | — |
| LE | 0.6 | 60.0 | 1.0x$10^{13}$ | 60.0 | 6.0x$10^{12}$ | 60.0 | 3.6x$10^{12}$ |
| Redhead | | 59.2 | — | 60.0 | — | 60.8 | — |
| LE | 0.8 | 60.0 | 1.0x$10^{13}$ | 60.0 | 4.0x$10^{12}$ | 60.0 | 1.6x$10^{12}$ |
| Redhead | | 59.7 | — | 60.0 | — | 60.3 | — |
| LE | 1.0 | 60.0 | 1.0x$10^{13}$ | 60.0 | 2.0x$10^{12}$ | 60.0 | 4.0x$10^{11}$ |
| Redhead | | 60.1 | — | 60.0 | — | 59.9 | — |

In table 2.1, we compare the obtained energies from Redhead and leading edge techniques for 0.2, 0.4, 0.6, 0.8 and 1.0 ML. For determining $E_{des}$ from the Redhead equation, the prefactor is set to 1x$10^{13}$ $s^{-1}$. In our simulation we have used 1000 data points per 1 K. We are aware that obtaining such high quality TPD data from an experiment is nearly impossible due to various reasons, i.e. QMS

sensitivity[15], experimental difficulties, etc. However, to compare the analysis techniques accurately, such a high quality simulation is essential.

Extracting desorption energies using the leading edge technique results in accurate results for the three different desorption orders (2.1). However, the pre-exponential factors obtained by this method change dramatically with the desorption order. For zero order desorption kinetics, it gives precise values for $E_{des}$ and $\nu_{des}$. However, for the first and second order desorption kinetics, it generates spurious results especially at large coverages. The Redhead model only seems accurate when desorption follows first order kinetics on the condition that a correct estimation for the prefactor is made. This is expected as this model is based on $T_M$, which is sufficiently constant at n = 1 (equation 2.1). Note that even for the first order desorption kinetics, an inaccurate $\nu_{des}$ can lead to incorrect desorption energies and prefactors. For example, the error introduced through a prefactor of $1x10^{12}$ $s^{-1}$ is more than 10 % for n = 1.

### 2.1.3 Complete analysis

The complete analysis yields coverage-dependent desorption energies. Applying the Polanyi-Wigner equation (equation 2.1) on a set of TPD spectra, $E_{des}$ and $\nu_{des}$ can be derived at a fixed coverage. This approach is generally useful for extracting kinetic information from single desorption features[11], where deconvolution of the TPD peaks is not required. In the following sections, we will elaborate more on this technique.

In figure 2.2a, we plotted the coverages versus the temperature for for n = 0, 1, and 2. The coverages are calculated by integrating each spectrum in figure 2.1. It is emphasised by dotted, horizontal lines that each spectrum has a different temperature and a different TPD rate at a certain coverage. When ln(r) vs. 1/T is plotted for each fixed coverage (0.1 - 0.8 ML), the slope and the intercept will yield $E_{des}$ and $\ln(\nu_{des})$ + n×ln(r), respectively. Figure 2.2b shows that the complete analysis technique produces more accurate $E_{des}$ and $\nu_{des}$ for zero, first and second order desorption, by comparison to previously mentioned methods (table 2.1).

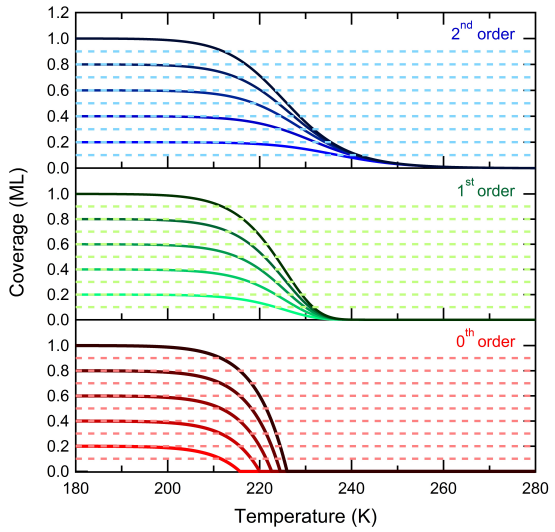


(a)

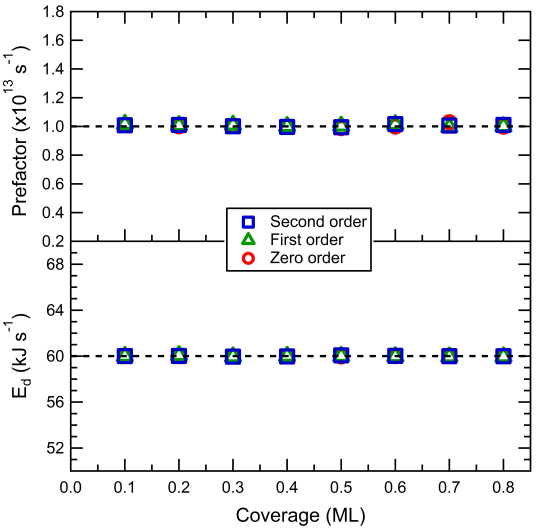


(b)

Figure 2.2: With complete analysis, coverage dependent $E_{des}$ and $\nu_{des}$ can be calculated. a) Coverages, obtained from figure 2.1, versus temperature for different desorption orders. The dotted lines indicates the fixed coverages. b) Calculated desorption energies and prefactors using complete analysis method for different desorption orders. The dotted lines are the simulated $E_{des}$ and $\nu_{des}$.

Although precise $E_{des}$ and $\nu_{des}$ can be derived from simulated data using complete analysis, a kinetic analysis of experimental TPD data is more complicated. For instance, low signal to noise ratio, non-integer desorption orders[10] and difficulties in background subtraction may strongly influence the accuracy of kinetic calculations. For the complete analysis method, the difficulties in obtaining a set of TPD spectra in a limited coverage regime[9] may result in a discontinuity in $E_{des}$ as a function of coverage. Also, most molecules give rise to a TPD spectrum with multiple desorption features. For the methods mentioned above, the analysis of TPD spectra with multiple peaks generally requires deconvolution, which may result in large errors, due to the difficulties in estimating the onset.

### 2.1.4 Inverse optimization

Tait et al.[16] have proposed an inverse optimization technique that yields accurate results when multiple desorption features are present in the TPD spectrum. Similar to complete analysis, this method also provides coverage dependent $E_{des}$. The prefactor, however, is not dependent on the coverage and the temperature. With the inverse optimization technique a continuous $E_{des}$ can be calculated as a function of coverage. The following expression (equation 2.6) is used for the inverse optimization technique for n = 1.

$$\mathrm{E}_{des}(\theta) = -\mathrm{RTln}[\frac{d\theta/dt}{\nu_{des}\theta}] \tag{2.6}$$

To illustrate this method, we show simulated TPD spectra with two desorption features in figure 2.3. For the high temperature peak, at $\sim$ 155 K, we fixed $E_{des}$ and $\nu_{des}$ at 40.0 kJ/mol and 1.0x10$^{13}$ s$^{-1}$, respectively. For the low temperature features, at 130 K, $E_{des}$ and $\nu_{des}$ are fixed at 30 kJ/mol and 1.0x10$^{11}$ s$^{-1}$, respectively. In our simulation for low and high temperature features, first and second order desorption kinetics are chosen, respectively.

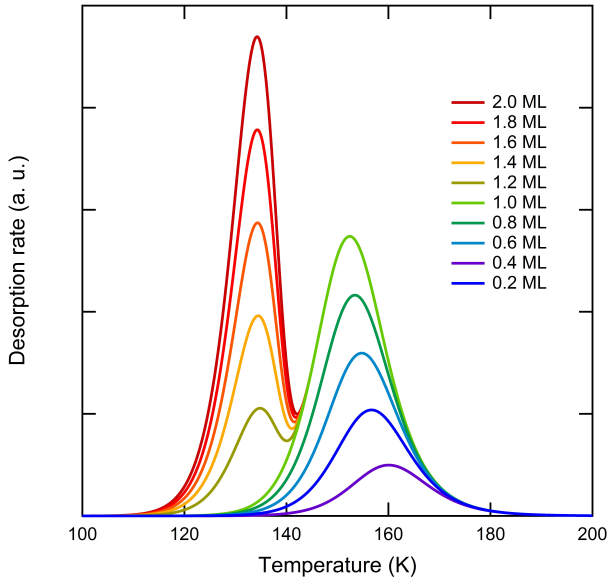


Figure 2.3: Simulated temperature programmed desorption spectra of adsorbing species for coverages up to 2.0 ML. We used first order desorption kinetics with $E_{des}$ = 30 kJ/mol and $\nu_{des}$ = 1.0x10$^{11}$ s$^{-1}$ for the low temperature features. For the high temperature peaks, we simulated the data with the following parameters: n = 2, $E_{des}$ = 40.0 kJ/mol and $\nu_{des}$ = 1.0x10$^{13}$ s$^{-1}$.

Similar to a TPD spectrum with a single desorption feature, the kinetics of the low temperature peak in figure 2.3 can be determined accurately using the leading edge analysis. Using the leading edge technique, we obtain an average desorption energy and prefactor of 30.0 kJ/mol and 1.0x10$^{11}$ s$^{-1}$. These values agree well with the tabulated results. In the following section we elucidate how the inverse optimization method can be applied to the high temperature peak.

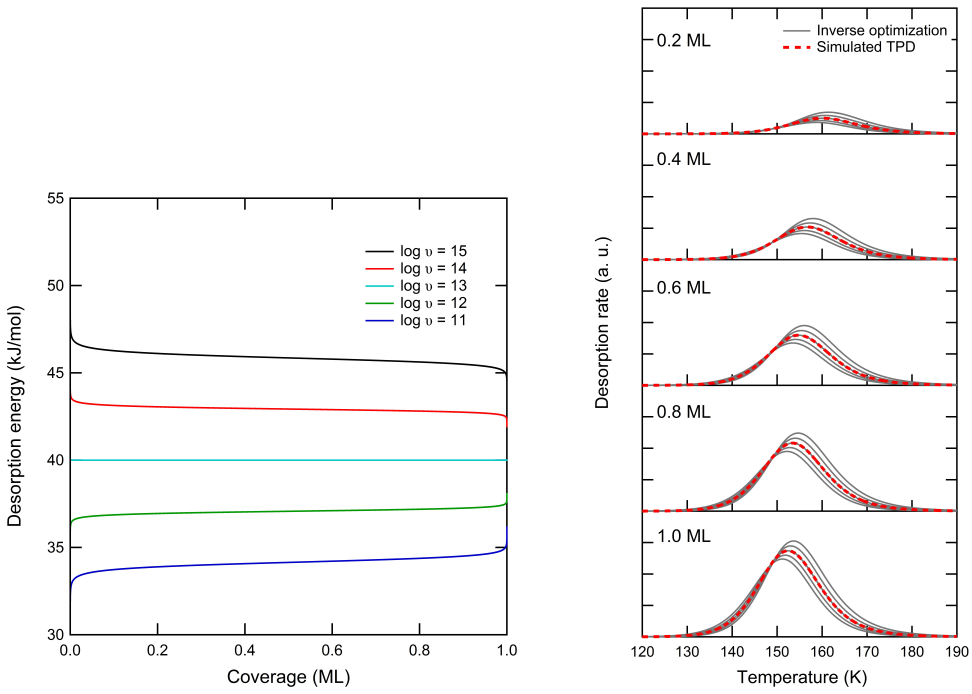


(a) (b)

Figure 2.4: Inverse optimization method[16] can provide a kinetic analysis with minimum discrete points. a) Equation 2.6 leads to various desorption energies when different approximations for the prefactor are made, $10^{11}$, $10^{12}$, $10^{13}$, $10^{14}$ and $10^{15}$ $s^{-1}$. b) TPD models (solid curves) derived from using the prefactors and corresponding $E_{des}$ shown in figure 2.4a. The dotted curves show simulated desorption features (figure 2.3) at 0.2, 0.4, 0.6, 0.8 and 1.0 ML.

Figure 2.4a displays coverage dependent desorption energies using equation 2.6 with different prefactors, $10^{11}$, $10^{12}$, $10^{13}$, $10^{14}$ and $10^{15}$ $s^{-1}$. Each energy plot is obtained using the Polanyi-Wigner equation (equation 2.1). Using the energy curves obtained in figure 2.4a, we created TPD models with different prefactors. In figure 2.4b, the generated TPD models (solid black curves) are compared with the high temperature features of the simulated data (red dotted curves) from figure 2.3. With this methodology, a reliable prefactor, which does not vary with $\theta$, can be determined.

To derive a quantitatively accurate prefactor, in figure 2.5 we have calculated a $\chi^2$ error between the modelled and simulated TPD spectra for each coverage in figure 2.4b. $\chi^2$ error is the sum of the squares of the leftovers compared to

simulation. The solid horizontal line in figure 2.5 expresses $\chi^2 = 0$. The dotted curve is a polynomial fit through the data, which reveal a minimum at $\log\nu_{des}$ = 13. As figure 2.4b also indicates, the most accurate prefactor calculated by inverse optimization method is $10^{13}$ $s^{-1}$. Therefore, the $E_{des}$ curve plotted in figure 2.4a for $\log\nu_{des} = 13$ (light blue) represents the actual coverage dependent desorption energy for the high temperature desorption feature (figure 2.3). Figure 2.4a shows that the obtained desorption energy is 40 kJ/mol, and does not change with increasing coverage. These results agree perfectly with the parameters set to generate the simulated data.

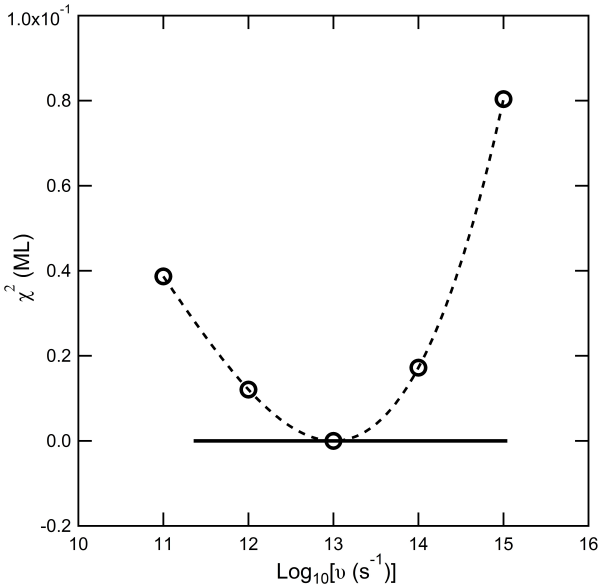


Figure 2.5: The $\chi^2$ error between the modelled and simulated TPD spectra as shown in figure 2.4b. The dotted line indicates the minimum of the polynomial fit (solid line) to the data.

## 2.2 Conclusions

To conclude, we have compared the most common methods to derive the activation energy and prefactor using very high quality TPD data. With leading edge analysis accurate $E_{des}$ for zero, first and second order desorption kinetics can be obtained when the spectrum consists of a single desorption feature. However, this method fails to derive a correct prefactor for n = 1 and 2. The Redhead analysis should generally be avoided as a small variation in estimating the prefactor may

cause a significant error. Finally, both complete analysis and inverse optimization method generate precise kinetic information. However, the latter yields continuous $E_{des}$ with no discrete points as a function of coverage. Therefore, it may be favored over complete analysis.

## 2.3 Bibliography

## References

(1) Niemantsverdriet, J., *Spectroscopy in Catalysis: An Introduction*; Wiley: 2000.

(2) Van der Niet, M. J. T. C.; Dominicus, I.; Koper, M. T. M.; Juurlink, L. B. F. *Physical Chemistry Chemical Physics* **2008**, *10*, 7169–7179.

(3) Van der Niet, M. J. T. C.; den Dunnen, A.; Juurlink, L. B. F.; Koper, M. T. M. *Journal of Chemical Physics* **2010**, *132*, 174705–174713.

(4) Van der Niet, M. J. T. C.; den Dunnen, A.; Juurlink, L. B. F.; Koper, M. T. M. *Physical Chemistry Chemical Physics* **2011**, *13*, 1629–1638.

(5) Smith, R. S.; May, R. A.; Kay, B. D. *The Journal of Physical Chemistry B* **2015**, *120*, 1979–1987.

(6) Pfnür, H; Feulner, P; Engelhardt, H.; Menzel, D *Chemical Physics Letters* **1978**, *59*, 481–486.

(7) Kolasinski, K. K.; Kolasinski, K. W., *Surface Science: foundations of catalysis and nanoscience*; John Wiley & Sons: 2012.

(8) Van Spronsen, M. A.; Weststrate, K.-J.; den Dunnen, A.; van Reijzen, M. E.; Hahn, C.; Juurlink, L. B. F. *The Journal of Physical Chemistry C* **2016**, acs.jpcc.6b00912.

(9) Badan, C.; Koper, M. T. M.; Juurlink, L. B. F. *The Journal of Physical Chemistry C* **2015**, *119*, 13551–13560.

(10) Radeke, M. R.; Carter, E. A. *Physical Review B* **1996**, *54*, 11803–11817.

(11) Nieskens, D.; van Bavel, A.; Niemantsverdriet, J. *Surface Science* **2003**, *546*, 159–169.

(12) Niemantsverdriet, J. W., *Spectroscopy in catalysis*; John Wiley & Sons: 2007.

(13) Redhead, P. A. *Vacuum* **1962**, *12*, 203–211.

(14) Habenschaden, E; Kuppers, J *Surface Science* **1984**, *138*, 147–150.

(15) Janlamool, J.; Bashlakov, D.; Berg, O.; Praserthdam, P.; Jongsomjit, B.; Juurlink, L. B. F. *Molecules* **2014**, *19*, 10845–10862.

(16) Tait, S. L.; Dohnalek, Z; Campbell, C. T.; Kay, B. D. *Journal of Chemical Physics* **2005**, *122*.